

2020-06

Hydrodynamic performance of a multi-Oscillating Water Column (OWC) platform

Zheng, Siming

<http://hdl.handle.net/10026.1/15626>

10.1016/j.apor.2020.102168

Applied Ocean Research

Elsevier

All content in PEARL is protected by copyright law. Author manuscripts are made available in accordance with publisher policies. Please cite only the published version using the details provided on the item record or document. In the absence of an open licence (e.g. Creative Commons), permissions for further reuse of content should be sought from the publisher or author.

Hydrodynamic performance of a multi-Oscillating Water Column (OWC) platform

Siming Zheng^{a,b}, Alessandro Antonini^c, Yongliang Zhang^d, Jon Miles^a, Deborah Greaves^a, Guixun Zhu^{a,*}, Gregorio Iglesias^{e,a}

a School of Engineering, Computing and Mathematics, University of Plymouth, Drake Circus, Plymouth PL4 8AA, UK

b State Key Laboratory of Coastal and Offshore Engineering, Dalian University of Technology, Dalian, 116024, China

c Department of Hydraulic Engineering, Delft University of Technology, The Netherlands

d State Key Laboratory of Hydroscience and Engineering, Tsinghua University, Beijing, 100084, China

e Centre for Marine and Renewable Energy Ireland (MaREI), Environmental Research Institute & School of Engineering, University College Cork, Ireland

<https://doi.org/10.1016/j.apor.2020.102168>

Received 27 December 2019

Received in revised form 26 March 2020

Accepted 15 April 2020

Hydrodynamic performance of a multi-Oscillating Water Column (OWC) platform

Siming Zheng^{a,b}, Alessandro Antonini^c, Yongliang Zhang^d, Jon Miles^a, Deborah Greaves^a, Guixun Zhu^{a,*}, Gregorio Iglesias^{e,a}

^a*School of Engineering, Computing and Mathematics, University of Plymouth, Drake Circus, Plymouth PL4 8AA, UK*

^b*State Key Laboratory of Coastal and Offshore Engineering, Dalian University of Technology, Dalian, 116024, China*

^c*Department of Hydraulic Engineering, Delft University of Technology, The Netherlands*

^d*State Key Laboratory of Hydroscience and Engineering, Tsinghua University, Beijing, 100084, China*

^e*MaREI, Environmental Research Institute & School of Engineering, University College Cork, Ireland*

Abstract

A rectangular barge consisting of multiple oscillating water columns (OWCs) is considered in this paper, hereinafter referred to as a multi-OWC platform. Each OWC chamber is enclosed by two partially submerged vertical walls and the deck of the platform. An incident wave produces oscillation of the water column in each OWC chamber and hence air is pumped by the internal water surface to flow through a Wells turbine installed at the chamber top. The effect of the turbine is characterised as a linear power take-off (PTO) system. A semi-analytical model based on linear potential flow theory and the eigen-function expansion method is developed to solve the wave radiation and diffraction problems of the multi-OWC platform. The hydrodynamic coefficients evaluated with direct and indirect methods of the model are shown to be in excellent agreement, and the energy conservation relationship of the multi-OWC platform is satisfied. The validated model is then applied to predict wave motion, dynamic air pressure, wave power extraction, and wave reflection and transmission coefficients of the multi-OWC platform. The effects of the PTO strategies, the number of chambers, the overall platform dimensions and the relative dimensions of adjacent

*Corresponding author. Email: guixun.zhu@plymouth.ac.uk

chambers on wave power extraction and wave attenuation are investigated. A smaller-draft front wall and a larger-draft back wall are found to be beneficial for broadening the range of high-efficiency performance of the platform. The same wave transmission coefficient can be obtained by two multi-OWC platforms with inverse geometric constructions.

Keywords: Marine renewable energy, Oscillating water columns, Wave power extraction, Wave transmission, Potential flow theory

1. Introduction

A large number of wave energy converters have been developed so far to capture energy from ocean waves. Among the large range of concepts for wave energy conversion, oscillating water columns (OWCs) are recognized as one of the most successful due to their mechanical and structural simplicity (He and Huang, 2014; Pereiras et al., 2015; Sheng, 2019; Zheng et al., 2019a,b). A typical OWC consists of a hollow chamber with its bottom opening to the sea below the waterline. As ocean waves propagate through the OWC, the water column enclosed by the chamber moves up and down, pumping the air in- and outside the chamber to flow through a turbine, which in turn drives a generator to produce electricity.

Until now, most studies of OWCs have been focused on single-chamber OWC devices. Falnes and McIver (1985) carried out a numerical study of an offshore two-dimensional (2D) single-chamber OWC device, the chamber of which was enclosed by two rigidly connected vertical thin barriers of unequal length. The resonance was found to occur not only at a frequency between the fundamental frequencies for water columns of length equal to the front and back barriers, but also at higher frequencies associated with the existence of standing waves between the barriers. In order to investigate the hydrodynamics of a nearshore single-chamber OWC device consisting of a thin vertical surface-piercing barrier in front of a vertical wall, Evans and Porter (1995) proposed an analytical model based on potential flow theory and a Galerkin method. The analytical re-

sults demonstrated that all incident wave power could be captured at resonance conditions. The effect of a stepped bottom topography in increasing the efficiency of such a nearshore single-chamber OWC was analytically, numerically and physically investigated by Rezanejad et al. (2013, 2016). While the OWC captures wave power from ocean waves, it also works similar to a breakwater to attenuate waves (He et al., 2017). Recently, He et al. (2019) investigated hydrodynamics of an offshore pile-supported OWC breakwater. Both wave power extraction and wave attenuation from the OWC breakwater were examined. It was found that both satisfactory power extraction and wave attenuation could be achieved by optimizing the power take-off (PTO) damping for maximum power.

In addition to the traditional single-chamber OWC, the concepts of dual-
35 and multi-chamber OWC devices were also proposed to improve wave power extraction by broadening the range of high-efficiency performance. Rezanejad et al. (2017) evaluated the wave power extraction from a nearshore dual-chamber OWC in finite water depth by using both analytical and numerical models. The draft of the outside chamber was found to be the dominant parameter in determining the basic resonance period that contributed to wave power absorption. The performance of the dual-chamber OWC with steps on the sea bed was analysed by Rezanejad et al. (2015). A wide frequency bandwidth in the computed range of wave periods was observed when the OWC was placed over the stepped sea bottom. Numerical and physical studies on dual-chamber OWC can also be found (He et al., 2013, 2017; Ning et al., 2018, 2019).
40 Noad and Porter (2017) proposed a simplified analytical study of an offshore multi-chamber OWC. Results showed that varying chamber size could lead to a broader-band power absorption efficiency response, and avoided the zeros in power absorption that occurred for equally-sized chambers. Note that their model is restricted by the assumptions of thin walls, shallow-draft, and infinite water depth.
45

In this paper, a stationary rectangular barge, which is composed of multiple OWCs is considered, hereinafter referred to as a multi-OWC platform (Fig.

1). A semi-analytical model of the multi-OWC platform is developed based
55 on linear potential flow theory and an eigen-function expansion method in the
absence of the thin-wall and the shallow draft assumptions, which were applied
in most of the previous analytical models of OWCs. This enables more details
of the properties of the platform to be captured, such as the effect of the thick-
ness and draft of the walls on the performance of the multi-OWC platform. An
60 obvious advantage of the semi-analytical model lies in its high computational
efficiency, which allows sensitivity analysis to be carried out for a large range of
parameters. Specifically, the effects of the PTO strategies, the number of cham-
bers, the overall platform dimensions and the relative dimensions of adjacent
chambers (width, thickness and draft of chamber walls) on the power extraction
65 of the multi-OWC platform are investigated.

The remainder of this paper is organized as follows. §2 presents mathematical
model for solving wave diffraction/radiation problem and evaluating wave
power extraction, wave reflection and transmission from the multi-OWC plat-
form. The convergence analysis and validation of the semi-analytical model can
70 be found in §3. §4 presents case studies of the multi-OWC chamber platform
with the employment of the validated semi-analytical model and discussion.
Finally, conclusions are drawn in §5.

2. Mathematical model

2.1. Problem description

75 As shown in Fig. 1, a stationary offshore multi-OWC platform is located
at the free-surface of the sea with the water depth h and water density ρ . A
Cartesian coordinate $Oxyz$ is adopted with the origin O in the mean water
level and Oz pointing vertically upwards. The length of the platform in the
70 Oy direction is assumed to be far longer than a wave length and there are no
intermediate walls along the Ox direction, so the hydrodynamic problem can be
treated in 2D. The platform is comprised of a series of N rectangular chambers
80 in the Ox direction, in which the n -th chamber is enclosed by the n -th and

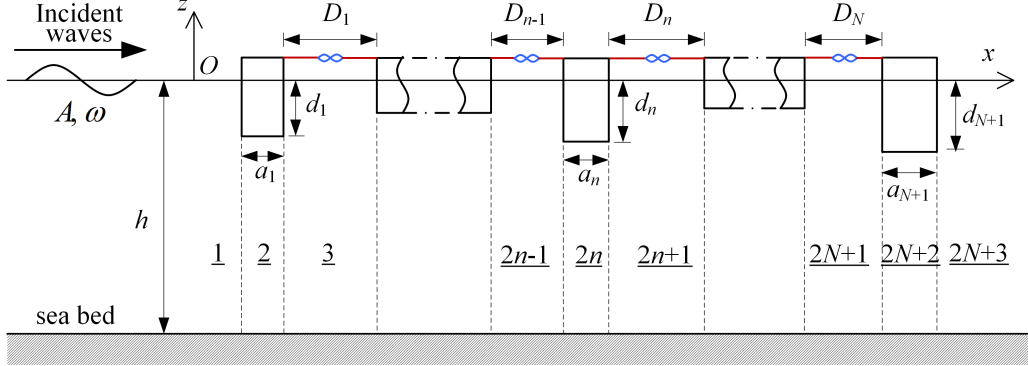


Figure 1: Side view of the multi-OWC platform.

$(n + 1)$ -th walls. The width of the n -th chamber is denoted as D_n , and the thickness and draft of the n -th wall are represented by a_n and d_n , respectively.
 85 As ocean waves propagate through the multi-OWC platform in the Ox -axis, the water column enclosed in each chamber rises and falls, causing an oscillating dynamic air pressure inside the chamber and in turn driving the air flow through a Wells turbine installed at the top of the chamber. It is assumed that the mass flux through the Wells turbine is proportional to the dynamic air pressure inside
 90 the OWC chamber and the effect of air compressibility in the chamber is linear (Sarmento and Falcão, 1985; Zheng et al., 2020). The effect of the Wells turbine in the n -th OWC chamber can be characterized as a linear damping, c_n . In this paper, regular incident waves with weak non-linearity are considered, and the amplitude and angular frequency are represented by A and ω , respectively.

95 2.2. Formulation of the wave diffraction/radiation problem

In common with the assumptions that have been employed by (Zheng and Zhang, 2016, 2018), the semi-analytical model developed in this paper is based on linearised hydrodynamic theory for an ideal irrotational fluid, and the deformation and motion of the platform are neglected. These assumptions have
 100 been adopted for the design of various wave energy converters, e.g., point absorber (Bozzi et al., 2013, 2017; Gaeta et al., 2020), raft-type device (Zheng

and Zhang, 2017) and OWC (Konispoliatis and Mavrakos, 2016, 2019).

The fluid motion can be expressed by the velocity potential $\Phi = \text{Re}[\phi(x, z)e^{-i\omega t}]$, where i is the imaginary unit, t is the time. ϕ is a complex spatial velocity potential satisfying the Laplace equation, and can be decomposed into an incident wave spatial potential ϕ_I , a diffracted wave spatial potential ϕ_0 , and N radiated wave spatial potentials:

$$\phi = \phi_I + \phi_0 + \sum_{L=1}^N p_L \phi_L, \quad (1)$$

where p_L is the complex amplitude of the dynamic air pressure above the internal air-water interface of the L -th OWC chamber; ϕ_L ($L = 1, 2, \dots, N$) is the corresponding spatial velocity potential due to unit oscillating dynamic air pressure inside the L -th OWC chamber in absence of incident waves.
105

An expression for ϕ_I , the dominating equation, and the boundary conditions that ϕ_0 should satisfy, can be found in our previous paper (Zheng and Zhang, 2016). Here, we only give the governing equation and boundary conditions that ϕ_L ($L = 1, 2, \dots, N$) should satisfy:

$$\frac{\partial^2 \phi_L}{\partial x^2} + \frac{\partial^2 \phi_L}{\partial z^2} = 0, \quad (2)$$

$$\frac{\partial \phi_L}{\partial z} - \frac{\omega^2}{g} \phi_L = \delta_{L,n} \frac{i\omega}{\rho g}, \quad z = 0, \quad x \in (-\infty, x_{l,1}) \cup (x_{r,n}, x_{l,n+1}) \cup (x_{r,N+1}) \quad (3)$$

$$\frac{\partial \phi_L}{\partial z} = 0, \quad z = -h, \quad (4)$$

$$\frac{\partial \phi_L}{\partial z} = -\delta_{L,0} \frac{\partial \phi_I}{\partial z}, \quad z = -d_n, \quad x \in (x_{l,n}, x_{r,n}), \quad (5)$$

$$\frac{\partial \phi_L}{\partial x} = -\delta_{L,0} \frac{\partial \phi_I}{\partial x}, \quad z \in (-d_n, 0), \quad x = x_{l,n} \text{ or } x_{r,n}, \quad (6)$$

in which $x_{l,n}$ and $x_{r,n}$ denote the positions of the left and right edges of the n -th wall in Ox -axis; δ denotes the Kronecker delta; g is the acceleration due to gravity. ϕ_L is outgoing with a finite value when $|x| = \infty$.

¹¹⁰ 2.3. Solution to diffracted/radiated potentials

To solve the wave diffraction and radiation problems, the fluid domain is divided into $2N+3$ subdomains denoted as Ω_n ($n = 1, 2, \dots, 2N+3$) as shown in Fig. 1. Utilizing the method of separation of variables, the analytical expressions for unknown ϕ_L ($L = 0, 1, 2, \dots, N$) in each subdomain, i.e., regions 1, $2n+1$, $2n$ and $2N+3$, can be expressed as follows (e.g., Zheng and Zhang (2016); Falnes (2002)):

$$\phi_1^{(L)} = \sum_{j=1}^{\infty} A_{1,j}^{(L)} e^{\lambda_j x} Z_j(z), \quad \text{in } \Omega_1, \quad (7)$$

$$\phi_{2n+1}^{(L)} = \sum_{j=1}^{\infty} (A_{2n+1,j}^{(L)} e^{\lambda_j x} + B_{2n+1,j}^{(L)} e^{-\lambda_j x}) Z_j(z) - \frac{i\delta_{L,n}}{\rho\omega}, \quad \text{in } \Omega_{2n+1}, \quad (8)$$

$$\phi_{2n}^{(L)} = -\delta_{L,0} \phi_I + A_{2n,1}^{(L)} x + B_{2n,1}^{(L)} + \sum_{j=2}^{\infty} (A_{2n,j}^{(L)} e^{\beta_{n,j} x} + B_{2n,j}^{(L)} e^{-\beta_{n,j} x}) \cos[\beta_{n,j}(z+h)], \quad \text{in } \Omega_{2n}, \quad (9)$$

$$\phi_{2N+3}^{(L)} = \sum_{j=1}^{\infty} A_{2N+3,j}^{(L)} e^{-\lambda_j x} Z_j(z), \quad \text{in } \Omega_{2N+3}, \quad (10)$$

in which $A_{1,j}^{(L)}$, $A_{2n+1,j}^{(L)}$, $B_{2n+1,j}^{(L)}$, $A_{2n,j}^{(L)}$, $B_{2n,j}^{(L)}$, and $A_{2N+3,j}^{(L)}$ are unknown coefficients to be determined; $\beta_{n,j}$ and λ_j are the eigen-values of the j -th wave modes in subdomain $2n$, and other subdomains, and Z_j is an eigen-function as:

$$\lambda_1 = -ik, \quad j = 1, \quad (11)$$

$$\omega^2 = -\lambda_j g \tan(\lambda_j h), \quad j = 2, 3, 4, \dots, \quad (12)$$

$$\beta_{n,j} = \frac{(j-1)\pi}{h - d_n}, \quad j = 2, 3, 4, \dots, \quad (13)$$

$$Z_j(z) = N_j^{-0.5} \cos[\lambda_j(h+z)], \quad N_j = 0.5 \left[1 + \frac{\sin(2\lambda_j h)}{2\lambda_j h} \right], \quad (14)$$

where k is the wave number satisfying $\omega^2 = gk \tanh(kh)$.

The continuity conditions of pressures or/and normal velocities at the interfaces between any two adjacent subdomains that should be satisfied by ϕ_L ($L = 0, 1, 2, \dots, N$) are presented as follows:

$$\frac{\partial \phi_{2n-1}^{(L)}}{\partial x} = \begin{cases} -\delta_{L,0} \frac{\partial \phi_I}{\partial x}, & x = x_{l,n}, z \in (-d_n, 0), \\ \frac{\partial \phi_{2n}^{(L)}}{\partial x}, & x = x_{l,n}, z \in (-h, -d_n), \end{cases} \quad (15)$$

$$\frac{\partial \phi_{2n+1}^{(L)}}{\partial x} = \begin{cases} -\delta_{L,0} \frac{\partial \phi_I}{\partial x}, & x = x_{r,n}, z \in (-d_n, 0), \\ \frac{\partial \phi_{2n}^{(L)}}{\partial x}, & x = x_{r,n}, z \in (-h, -d_n), \end{cases} \quad (16)$$

$$\phi_{2n-1}^{(L)} = \phi_{2n}^{(L)} \quad x = x_{l,n}, z \in (-h, -d_n), \quad (17)$$

$$\phi_{2n}^{(L)} = \phi_{2n+1}^{(L)} \quad x = x_{r,n}, z \in (-h, -d_n), \quad (18)$$

Upon substituting Eqs. (7)–(10) for ϕ_L in different subdomains into these continuity conditions Eqs. (15)–(18), utilizing the orthogonality relations of the integration of eigen-functions over the vertical dimension and taking the first 115 M terms in the infinite series, a linear system of $4(N + 1)M$ complex equations for each ϕ_L with the same number of unknown coefficients are obtained. The unknown coefficients can be easily evaluated by solving a $4(N + 1)M$ -order linear matrix equation (Zheng and Zhang, 2016, 2018).

2.4. Hydrodynamic coefficients due to wave diffraction and radiation

120 2.4.1. Direct Method (DM) for solving hydrodynamic coefficients

The upward flux at the water surface inside the n -th OWC chamber due to the contributions of undisturbed incident wave and the diffracted wave, the so-called wave excitation volume flux, can be written as $\text{Re}[F_e^{(n)} e^{-i\omega t}]$,

$$F_e^{(n)} = \int_{x_{r,n}}^{x_{l,n+1}} \frac{\partial(\phi_I + \phi_0)}{\partial z} |_{z=0} dx. \quad (19)$$

The complex amplitude of the upward flux at the water surface inside the n -th OWC chamber due to the radiated waves induced by the oscillations of

the OWC chambers can be written as

$$\begin{aligned}
F_R^{(n)} &= \int_{x_{r,n}}^{x_{l,n+1}} \partial \left(\sum_{L=1}^N p_L \phi_L \right) / \partial z |_{z=0} dx \\
&= \frac{\omega^2}{g} \sum_{L=1}^N p_L \sum_{j=1}^{\infty} \left[A_{2n+1}^{(L)} (e^{\lambda_j x_{l,n+1}} - e^{\lambda_j x_{r,n}}) - B_{2n+1}^{(L)} (e^{-\lambda_j x_{l,n+1}} - e^{-\lambda_j x_{r,n}}) \right] \frac{Z_j(0)}{\lambda_j} \\
&= \sum_{L=1}^N p_L (i\mu_{n,L} - c_{n,L}),
\end{aligned} \tag{20}$$

where $\mu_{n,L}$ and $c_{n,L}$ are the so-called radiation susceptance (added-mass) and radiation conductance (wave radiation damping), respectively,

$$\mu_{n,L} = \frac{\omega^2}{g} \text{Im} \sum_{j=1}^{\infty} \left[A_{2n+1}^{(L)} (e^{\lambda_j x_{l,n+1}} - e^{\lambda_j x_{r,n}}) - B_{2n+1}^{(L)} (e^{-\lambda_j x_{l,n+1}} - e^{-\lambda_j x_{r,n}}) \right] \frac{Z_j(0)}{\lambda_j}, \tag{21}$$

$$c_{n,L} = -\frac{\omega^2}{g} \text{Re} \sum_{j=1}^{\infty} \left[A_{2n+1}^{(L)} (e^{\lambda_j x_{l,n+1}} - e^{\lambda_j x_{r,n}}) - B_{2n+1}^{(L)} (e^{-\lambda_j x_{l,n+1}} - e^{-\lambda_j x_{r,n}}) \right] \frac{Z_j(0)}{\lambda_j}. \tag{22}$$

2.4.2. Indirect method for solving hydrodynamic coefficients

Apart from using the direct method, the excitation volume flux may also be expressed in terms of the radiated wave's far-field coefficients using the Haskind Relation (HR) as:

$$F_e^{(n)} = \frac{2i\rho g Akh A_{1,1}^{(n)}}{Z_1(0)}, \tag{23}$$

Similarly, with the employment of the Haskind Relation (HR), $c_{n,L}$ can be written in terms of the radiated wave's far-field coefficients as follows

$$c_{n,L} = \omega \rho kh (A_{2N+3,1}^{(n)*} A_{2N+3,1}^{(L)} + A_{1,1}^{(n)*} A_{1,1}^{(L)}), \tag{24}$$

where the superscript * denotes complex-conjugate.

¹²⁵ 2.5. Wave power absorption

After solving the wave diffraction/radiation problem and obtaining the hydrodynamic coefficients, the water column motion response of the multi-OWC platform in the frequency domain can be calculated by the equation:

$$[-i(\mathbf{M}_a + \mathbf{M}_{PTO}) + (\mathbf{C}_d + \mathbf{C}_{PTO})]\dot{\mathbf{X}} = \mathbf{F}_e, \quad (25)$$

where \mathbf{M}_a and \mathbf{C}_d are the matrices of $\mu_{n,L}$ and $c_{n,L}$, respectively; \mathbf{C}_{PTO} denotes a diagonal damping matrix induced by the PTO system (i.e., turbines) (Sarmento and Falcão, 1985); \mathbf{M}_{PTO} represents a diagonal matrix adopted to consider the effect of air compressibility, where the n -th element in the diagonal can be expressed as $\mu_{PTO}^{(n)} = \omega V_n / (v^2 \rho_0)$, in which V_n is the air chamber volume of the n -th OWC, v denotes the speed of sound in air and ρ_0 represents the static air density. In this paper, the platform deck is assumed 0.2h above the mean water level, hence $V_n = 0.2hD_n$ is adopted. $\dot{\mathbf{X}} = [p_1 \ p_2 \ \cdots \ p_N]^T$ is the dynamic air pressure response vector of the multi-OWC platform to be determined, where the superscript T denotes the transpose; \mathbf{F}_e is the wave excitation volume flux vector.

The time averaged wave power absorbed by the multi-OWC platform can be evaluated by

$$P = \frac{1}{2} \sum_{n=1}^N c_n |p_n|^2. \quad (26)$$

The wave power absorption efficiency is defined as

$$\eta = \frac{P}{0.5\rho g A^2 c_g}, \quad (27)$$

where the denominator denotes the incident wave power, in which c_g represents the wave group velocity.

2.6. Wave reflection and transmission coefficients

The wave reflection coefficient and the wave transmission coefficient of the multi-OWC platform, denoted as $R = |\hat{R}|$ and $T = |\hat{T}|$, respectively, in which \hat{R}

and \hat{T} are the corresponding complex amplitudes of the coefficients calculated as:

$$\hat{R} = \frac{\omega}{gA} Z_1(0) (A_{1,1}^{(0)} + \dot{\mathbf{X}}^T \mathbf{A}^-), \quad (28)$$

$$\hat{T} = \hat{T}_0 + \frac{i\omega}{gA} Z_1(0) \dot{\mathbf{X}}^T \mathbf{A}^+ = 1 + \frac{i\omega}{gA} Z_1(0) (A_{2N+3,1}^{(0)} + \dot{\mathbf{X}}^T \mathbf{A}^+), \quad (29)$$

where $\mathbf{A}^- = [A_{1,1}^{(1)} \ A_{1,1}^{(2)} \ \cdots \ A_{1,1}^{(N)}]^T$, $\mathbf{A}^+ = [A_{2N+3,1}^{(1)} \ A_{2N+3,1}^{(2)} \ \cdots \ A_{2N+3,1}^{(N)}]^T$, and \hat{T}_0 represents the complex transmission coefficient of the multi-OWC platform without any deck (i.e., no dynamic air pressure exist inside each OWC chamber).

3. Convergence analysis and model validation

In the following sections, the hydrodynamic quantities, together with the parameters associated with PTO system, are nondimensionalized by

$$\bar{F}_e^{(j)} = \frac{|F_e^{(j)}|}{A\sqrt{gh}}, \quad \{\bar{c}_{i,j}, \bar{\mu}_{i,j}, \bar{c}_{\text{PTO}}^{(j)}, \bar{\mu}_{\text{PTO}}^{(j)}\} = \frac{\rho g}{\sqrt{gh}} \{c_{i,j}, \mu_{i,j}, c_{\text{PTO}}^{(j)}, \mu_{\text{PTO}}^{(j)}\}. \quad (30)$$

3.1. Convergence analysis

A convergence analysis is performed for a multi-OWC platform with $h=10$ m, $a_1/h=a_2/h=a_3/h=0.05$, $D_1/h=0.5$, $D_2/h=0.8$, $d_1/h=0.1$, $d_2/h=0.2$, $d_3/h=0.3$, $x_{l,1}=0.0$ in waves of kh ranging from 0.05 to 10. Figs. 2 and 3 illustrate the impact of vertical truncated cut-offs (i.e., the number of the first terms truncated in the infinite series of eigen-functions, in terms of M) on $\bar{F}_e^{(1)}$, $\phi_e^{(1)}$, $\bar{c}_{1,1}$ and $\bar{\mu}_{1,1}$, in which $\phi_e^{(1)}$ represents the phase of $F_e^{(1)}$. It can be seen from Fig. 2 for a wide range of wave frequencies and Fig. 3 for $kh = 3.0$ that convergence is achieved when $M \geq 20$ is used.

The variation of the CPU time required for the simulation of 100 wave frequencies with the vertical truncated cut-offs in terms of M is plotted in Fig. 3 as well. The CPU time is found to increase more and more quickly with the increase of the vertical truncated cut-offs. In order to obtain converged results and, meanwhile, to ensure high computational efficiency of the semi-analytical model, $M = 20$ is adopted hereinafter.

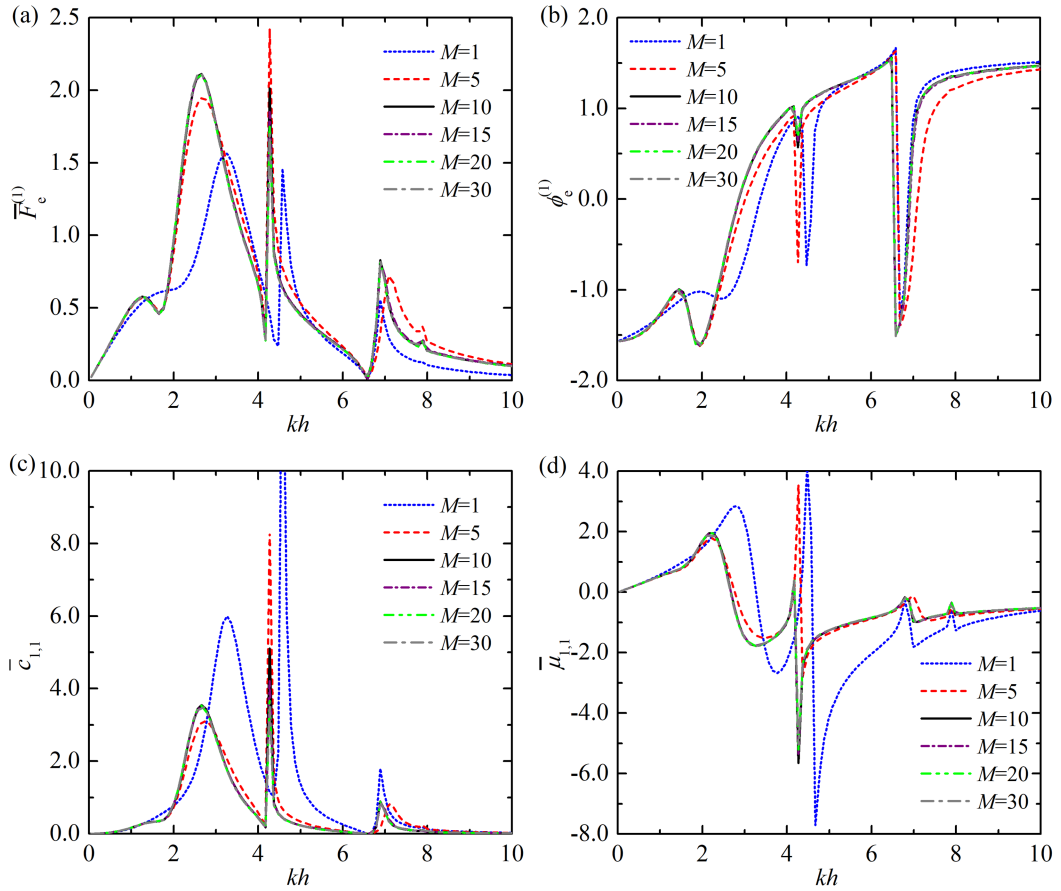


Figure 2: Impact of the vertical cut-offs (i.e., in terms of M) on (a) $\bar{F}_e^{(1)}$; (b) $\phi_e^{(1)}$; (c) $\bar{c}_{1,1}$; (d) $\bar{\mu}_{1,1}$.

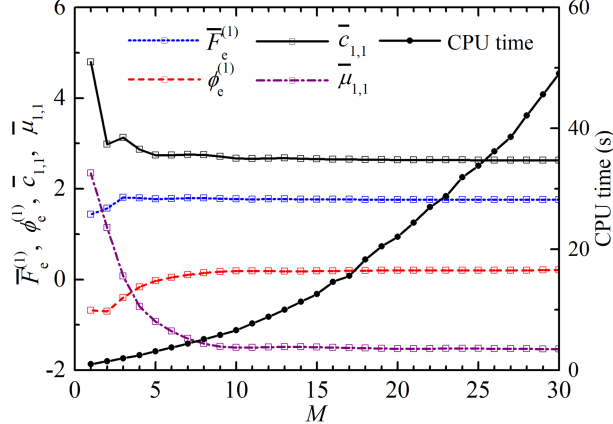


Figure 3: Variation of $\bar{F}_e^{(1)}$, $\bar{\phi}_e^{(1)}$, $\bar{c}_{1,1}$, $\bar{\mu}_{1,1}$, and the CPU time required for the simulation of 100 wave frequencies with the number of cut-offs (i.e., in terms of M). [$kh=3.0$, $h=10$ m, $a_1/h=a_2/h=a_3/h=0.05$, $D_1/h=0.5$, $D_2/h=0.8$, $d_1/h=0.1$, $d_2/h=0.2$, $d_3/h=0.3$, $x_{l,1}=0.0$]

3.2. Model validation

To validate the semi-analytical model for solving wave diffraction/radiation problems as described in §2, wave excitation volume flux and hydrodynamic coefficients are evaluated by using both the direct method and indirect method. Fig. 4 presents the comparison between these results for $N=2$, $h=10$ m, $a_1/h=a_2/h=a_3/h=0.05$, $D_1/h=0.5$, $D_2/h=0.8$, $d_1/h=0.1$, $d_2/h=0.2$, $d_3/h=0.3$. Additionally, the results of η , R , T and $\eta + R^2 + T^2$ for the same platform with $\mathbf{C}_{\text{PTO}} = \text{diag}(\mathbf{C}_d)$ is illustrated in Fig. 5.

Figs. 4 and 5 show that the results of wave excitation volume flux and hydrodynamic coefficients by using two different methods are in excellent agreement and the energy conservation relationship, i.e., $\eta + R^2 + T^2 = 1$, is satisfied perfectly. The “reciprocity” relation between the wave radiation damping/added-masses, i.e., $\bar{c}_{1,2} = \bar{c}_{2,1}$ and $\bar{\mu}_{1,2} = \bar{\mu}_{2,1}$, is also demonstrated (Figs. 4d and 4f). This gives confidence in the present semi-analytical model for solving wave diffraction/radiation problems and evaluating wave power absorption, wave reflection/transmission of the multi-OWC platform.

Note from Fig. 5 that a peak of wave power absorption occurs around

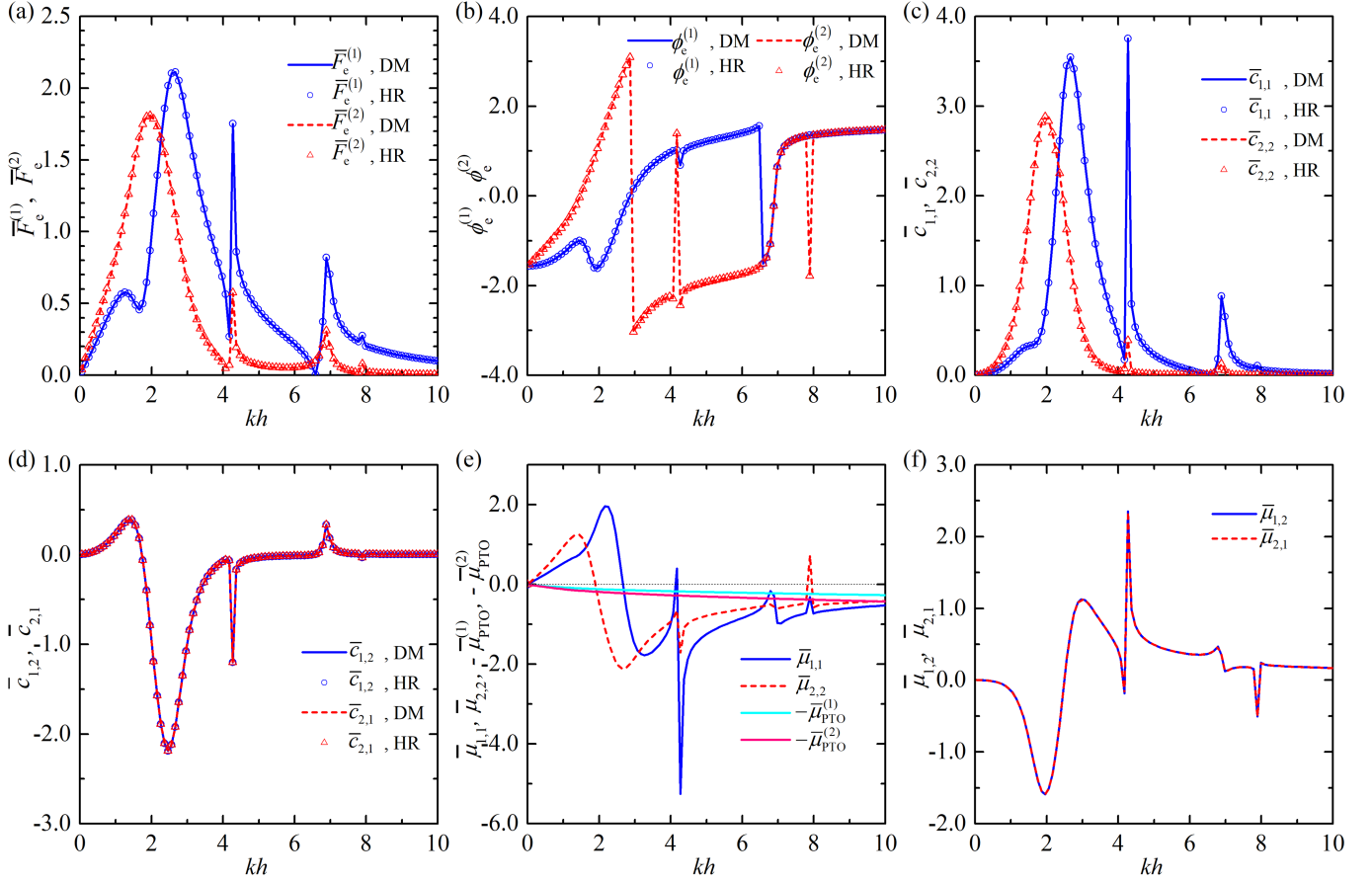


Figure 4: Wave excitation volume flux and hydrodynamic coefficients: (a) $\bar{F}_e^{(1)}$ and $\bar{F}_e^{(2)}$; (b) $\phi_e^{(1)}$ and $\phi_e^{(2)}$; (c) $\bar{c}_{1,1}$ and $\bar{c}_{2,2}$; (d) $\bar{c}_{1,2}$ and $\bar{c}_{2,1}$; (e) $\bar{\mu}_{1,1}$, $\bar{\mu}_{2,2}$, $\bar{\mu}_{\text{PTO}}^{(1)}$, and $\bar{\mu}_{\text{PTO}}^{(2)}$; (f) $\bar{\mu}_{1,2}$ and $\bar{\mu}_{2,1}$. [$N=2$, $h=10$ m, $a_1/h=a_2/h=a_3/h=0.05$, $D_1/h=0.5$, $D_2/h=0.8$, $d_1/h=0.1$, $d_2/h=0.2$, $d_3/h=0.3$, $x_{l,1}=0.0$]

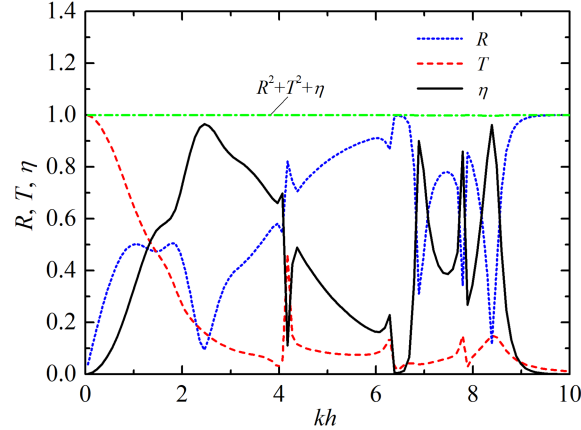


Figure 5: Frequency responses of wave reflection and transmission coefficients, and wave power absorption efficiency. [$N=2$, $h=10$ m, $a_1/h=a_2/h=a_3/h=0.05$, $D_1/h=0.5$, $D_2/h=0.8$, $d_1/h=0.1$, $d_2/h=0.2$, $d_3/h=0.3$, $x_{l,1}=0.0$]

$kh=2.5$. In order to demonstrate how wave motion is affected by the multi-OWC platform in this wave condition, the corresponding instantaneous water elevation at different times is illustrated in Fig. 6, where the water elevation response around vertical surface-piercing barriers (i.e., the platform with no deck) and a closed multi-chamber platform (i.e., the platform with a completely sealed deck) is plotted as well as a comparison. Standing waves are observed for both the vertical surface-piercing barriers and closed multi-chamber platform situations, while the anti-nodes positions are different (Figs. 6a and 6b), meaning that the waves reflected from them are almost as strong as the incident waves. The oscillation of the water columns between the vertical surface-piercing barriers are dramatic in the absence of any restriction of dynamic air pressure. On the contrary, there are nearly no wave motion inside the chambers of the closed multi-chamber platform due to the existence of the sealed deck. In spite of this, waves are still partly transmitted to the back of the closed multi-chamber platform, yet slightly less than those of the surface-piercing barriers.

For the multi-OWC platform (Fig. 6c), there are almost no waves reflected from it, and, meanwhile, the transmitted waves are obviously weaker compared

with the other two circumstances. It means that, for $kh=2.5$, the multi-OWC platform is capable of absorbing most of the incident power, and significantly attenuating waves at the same time.

4. Results and discussion

The performance of the multi-OWC platform in terms of wave power extraction and wave attenuation depends upon several parameters: the PTO strategies, the width of each chamber, the thickness and the draft of each wall, and the number of chambers. Hereinafter, the walls and chambers of the platform are assumed identical, i.e., $a_j=a_n$, $d_j=d_n$ and $D_j=D_n$, unless otherwise specified. The overall length of the platform in the Ox direction is denoted as l_0 , i.e., $l_0=x_{r,N+1} - x_{l,1}$. The effect of multiple parameters on wave power extraction and wave transmission is examined in this section.

4.1. Effect of PTO strategies

Following Bellew et al. (2009), three PTO strategies are considered, i.e., $\mathbf{C}_{\text{PTO}} = \text{diag}(\mathbf{C}_d)$, $\mathbf{C}_{\text{PTO}} = \text{diag}([\mathbf{C}_d^2 + (\mathbf{M}_a + \mathbf{M}_{\text{PTO}})^2]^{0.5})$, $\mathbf{C}_{\text{PTO}} = \mathbf{C}_{\text{opt}}$, in which \mathbf{C}_{opt} represents a diagonal matrix with all elements non-negative that maximizes power absorption of the multi-OWC platform.

Fig. 7 presents the power absorption efficiency and wave transmission coefficient of the platform with these three different PTO strategies for $N=2$, $h=10$ m, $l_0/h=2.0$, $a_j/h=0.05$, and $d_j/h=0.2$. There is a main peak of the $\eta-kh$ curve and it occurs around $kh=1.6$ regardless of the PTO strategy adopted. The peak values corresponding to the three PTO strategies are 0.74, 0.73 and 0.83, respectively. Some other peaks are observed at higher wave frequencies, e.g., $kh=3.8$ and 6.9. Note that at $kh=6.8$, the multi-OWC platform absorbs almost no wave power and also does not transmit the incident wave, such that the incident wave is completely reflected by the platform. The incident wave is completely reflected by the platform. For such wave condition, $kD_j = 2\pi$ is satisfied, i.e., the width of the water column in each chamber is equal to the

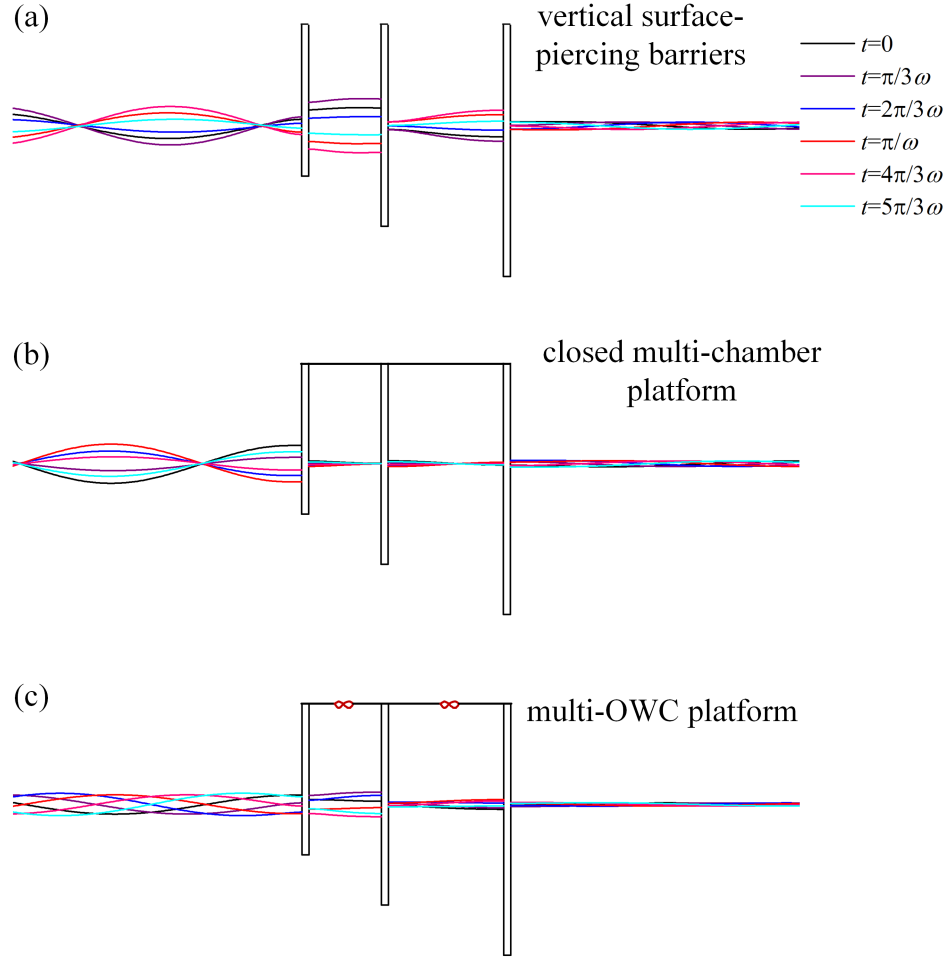


Figure 6: Instantaneous water elevation at different times: (a) vertical surface-piercing barriers; (b) closed multi-chamber platform; (c) multi-OWC platform. [Incident waves incoming from the left-hand side. $N=2$, $kh = 2.5$, $h=10$ m, $a_1/h=a_2/h=a_3/h=0.05$, $D_1/h=0.5$, $D_2/h=0.8$, $d_1/h=0.1$, $d_2/h=0.2$, $d_3/h=0.3$, $x_{l,1}=0.0$]

wavelength, hence no wave excitation volume flux can be excited, resulting in zero wave power absorption.

As expected, the corresponding η for Strategy 3 is found to be no less than that of any other two PTO strategies for the entire range of the computed wave conditions. Although the main peak value of η for Strategy 2 is slightly smaller than that for Strategy 1, the performance of the platform with Strategy 2 is closer to the optimized one (i.e., with Strategy 3) for most of the remaining wave frequencies. Moreover, Strategy 2 performs much better than the other strategies in wave attenuation for a certain range of wave conditions, e.g., $kh \in$ 230 (4.0, 8.0).

For $N=2$, the \mathbf{C}_{opt} adopted in Strategy 3 can be obtained by using an analytical method (Zheng and Zhang, 2018), and for the platform consisting of more chambers, i.e., $N=3, 4, \dots$, \mathbf{C}_{opt} can be found by applying numerical iterations, e.g., a trial and error (“brute force”) method, which might be prohibitively 235 time consuming and/or lead to inaccurate results. Hereinafter, Strategy 2, i.e., $\mathbf{C}_{\text{PTO}} = \text{diag}([\mathbf{C}_d^2 + (\mathbf{M}_a + \mathbf{M}_{\text{PTO}})^2]^{0.5})$, which is more straightforward than Strategy 3 and meanwhile gives better power absorption and wave attenuation for most wave conditions than Strategy 1, is employed.

4.2. Effect of the number of chambers

240 Fig. 8 presents the frequency response of the power absorption efficiency and wave transmission coefficient of the multi-OWC platform ($h=10$ m, $l_0/h=2.0$, $a_j/h=0.05$, $d_j/h=0.2$) with different numbers of chambers. Since the overall length and thickness of each wall are both fixed, more chambers mean smaller width of each OWC chamber.

245 As the platform changes from the single-OWC to the dual-OWC (i.e., from $N=1$ to $N=2$, see Fig. 8), the wave power extraction from the platform is significantly improved in terms of both a larger peak value and a larger bandwidth of the main $\eta-kh$ peak, meanwhile, the wave transmission is dramatically repressed. As N increases towards $N = 5$ power extraction continues to improve 250 although at a reducing rate of improvement. For long waves, e.g., $kh \in (0, 0.5)$,

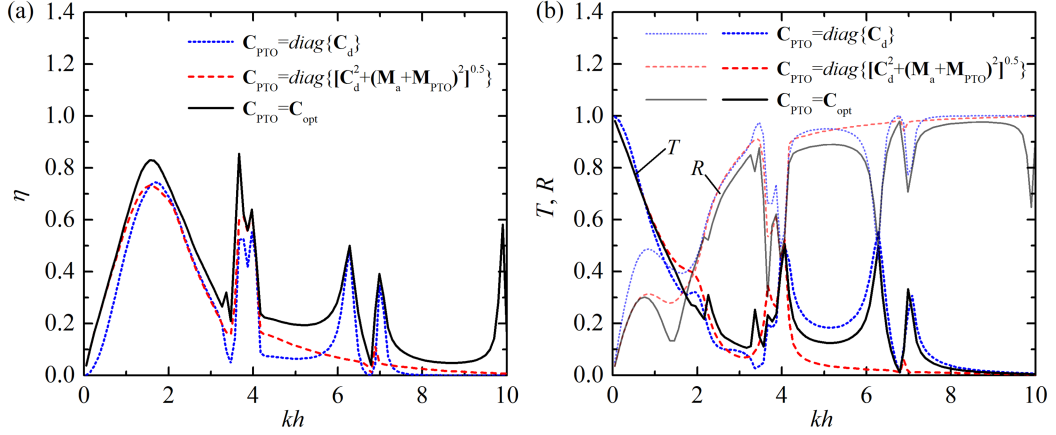


Figure 7: Frequency response of wave power absorption efficiency, wave reflection and transmission coefficients for different PTO strategies: (a) η ; (b) R and T . [$N=2$, $h=10$ m, $l_0/h=2.0$, $a_j/h=0.05$, $d_j/h=0.2$]

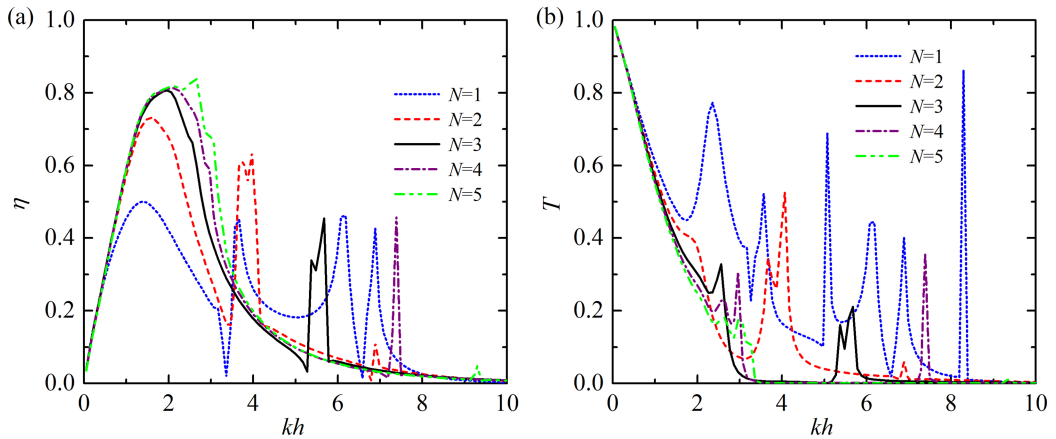


Figure 8: Frequency response of wave power absorption efficiency and wave transmission coefficient for different number of chambers, i.e., N : (a) η ; (b) T . [$h=10$ m, $l_0/h=2.0$, $a_j/h=0.05$, $d_j/h=0.2$]

η and T are found to be independent of N . This is because the piston-like motion of the water column dominates all along the platform in long waves and the introduction of intermediate walls does not matter. As N increases, all the peaks of the $\eta-kh$ curves shift towards larger wave frequencies as illustrated in Fig. 8, and this is induced by the larger resonance frequencies for the smaller-width OWC chambers. As discussed in §4.1, for the wave condition where $kD_j = 2\pi$ is satisfied, there are nearly no power can be captured by the platform. This applies to the results plotted in Fig. 8a as well. In the computed range of kh , there are two wave conditions with no power absorbed for $N=1$, i.e., $kh=3.3$ and 6.6 , which correspond to $kD_j=2\pi$ and 4π , respectively. The multi-OWC platforms with $N=4$ and 5 rarely transmit the short incident waves, e.g., $kh \in (3.4, 10)$ (Fig. 8b).

Applying more chambers could obviously enhance power capture and wave attenuation ability of the multi-OWC platform. However, it requires more PTO units and more internal walls, which in turn leads to higher costs of construction and maintenance. $N=2$ or 3 might be the best option in practice with the trade-off between the power extraction/wave attenuation and costs.

4.3. Effect of the overall platform length

Fig. 9 illustrates the frequency response of the wave power absorption efficiency and wave transmission coefficient of the multi-OWC platform with different overall length for $N=2$, $h=10$ m, $a_j/h=0.05$ and $d_j/h=0.2$. For the platform consisting of two chambers with the size of each wall fixed, increasing the overall platform length is achieved by broadening width of each OWC chamber.

As illustrated in Fig. 9, the peaks of the $\eta-kh$ and $T-kh$ curves shift towards the smaller wave frequencies with the increase of l_0/h . This is reasonable from the view of compatibility between incident wave length and OWC chamber width. More specifically, the OWC chamber with a larger width (i.e., l_0/h) is more likely to reach the resonance in longer waves (i.e., smaller kh). For kh ranging from 0 to 2.0, the longer of l_0/h , the smaller of T . Note that the peak values of η increase with l_0/h ; meanwhile, the two kh values corresponding to

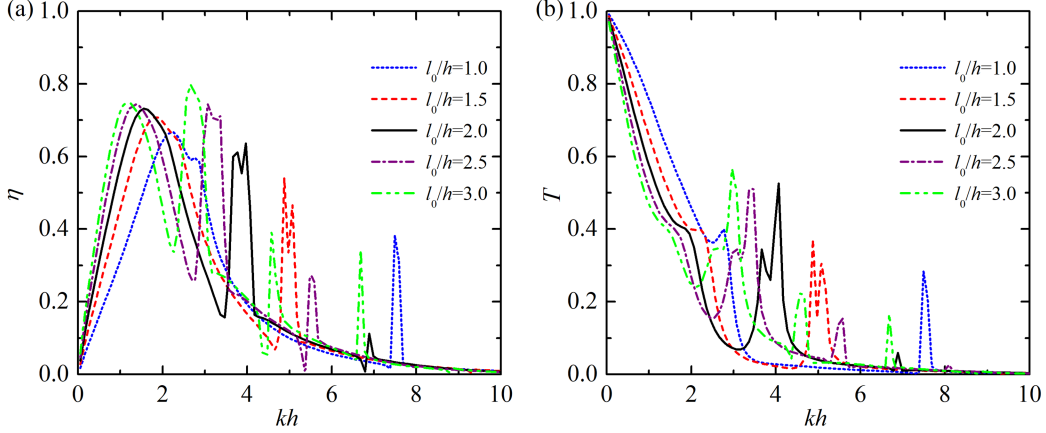


Figure 9: Frequency response of wave power absorption efficiency and wave transmission coefficient for different overall platform length, i.e., l_0/h : (a) η ; (b) T . [$N=2$, $h=10$ m, $a_j/h=0.05$, $d_j/h=0.2$]

the first two peaks are closer together, making the platform more and more sensitive to kh in a specified range of wave frequencies. In the computed range of wave conditions, there are four peaks of the η - kh curve observed for $l_0/h=3.0$, whereas only three or even two are found for $l_0/h=1.0, 1.5, 2.0$, and 2.5 . Similar change is also observed for the T - kh curve (Fig. 9b). These peaks are associated with resonances of the multi-OWC platform. For a multi-OWC platform with identical chambers, the resonances might be calculated by satisfying $\mu_{1,1} - \mu_{\text{PTO}}^{(1)} \rightarrow 0$. The larger the value of l_0/h , more resonances are likely to occur in a specified range of wave frequencies.

290 4.4. Effect of the wall thickness

The effect of the wall thickness (i.e., a_j) on wave power extraction and wave transmission is investigated by examining the performance of the platform with the employment of $a_j/h = 0.01, 0.03, 0.05, 0.07$, and 0.09 for $N=2$, $h=10$ m, $l_0/h=2.0$ and $d_j/h=0.2$. Results for these five cases are illustrated in Fig. 10.

295 The main peak of the η - kh curve is found to be slightly weakened in terms of both peak value and bandwidth with the increase of a_j/h (Fig. 10a). The kh

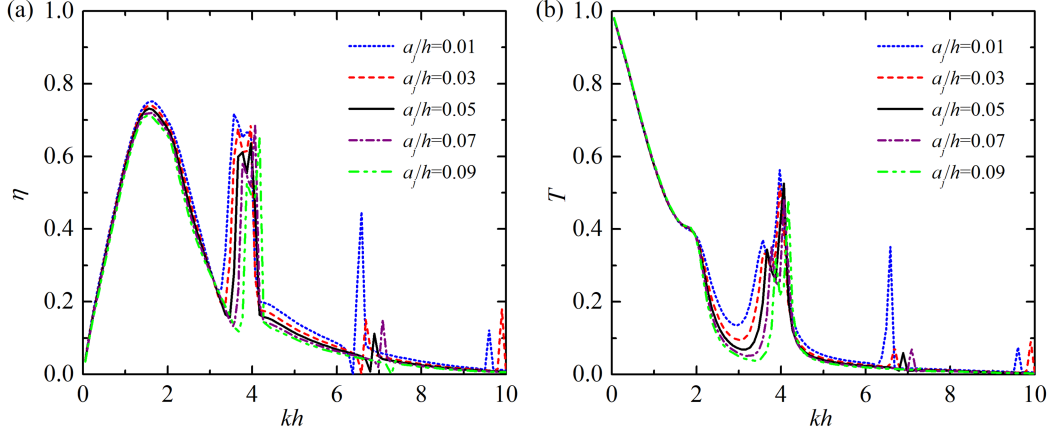


Figure 10: Frequency response of wave power absorption efficiency and wave transmission coefficient for different wall thickness, i.e., a_j/h : (a) η ; (b) T . [$N=2$, $h=10$ m, $l_0/h=2.0$, $d_j/h=0.2$]

where the main peak occurs seems to be independent of a_j/h . The other peaks at high wave frequencies are found sensitive to the change of a_j/h . The larger the value of a_j/h , the narrower and smaller of these peaks, and the larger the kh where these peaks occur. As a_j/h increases, the corresponding D_j/h decreases, resulting in a larger kh where no power absorption ($kD_j = 2\pi$) occurs.

As shown in Fig. 10b, for $kh \in (0, 2.0)$, wave attenuation of the multi-OWC platform is not affected by the change of the wall thickness. As kh increases, a_j/h starts playing a role in influencing wave transmission, the thicker the wall, the smaller the value of T , and such a role reaches its strongest at $kh \in (2.5, 4.0)$.

It is shown in Fig. 10 that the multi-OWC platform with thinner walls is welcome for the better performance in terms of wave power extraction for most of the computed range of kh ; however, from the view of wave attenuation, the multi-OWC platform with thicker walls becomes a better choice since smaller values of T are generally obtained.

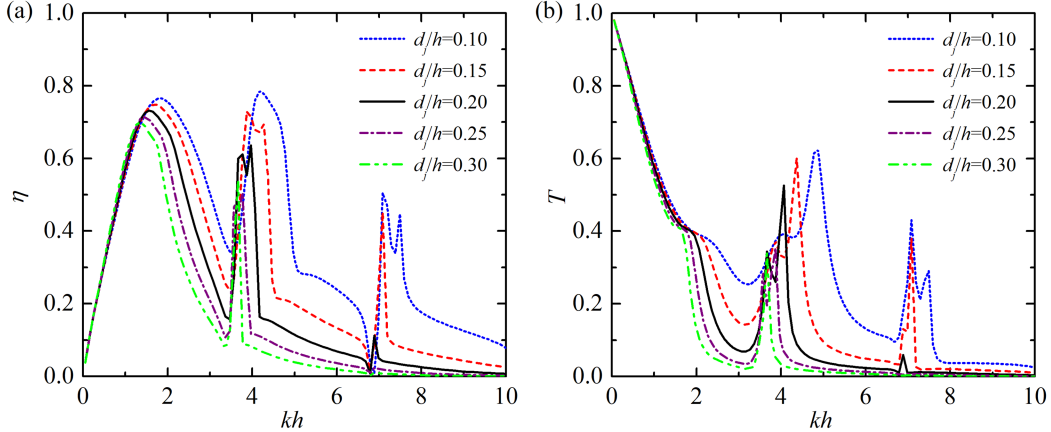


Figure 11: Frequency response of wave power absorption efficiency and wave transmission coefficient for different wall draft, i.e., d_j/h : (a) η ; (b) T . [$N=2$, $h=10$ m, $l_0/h=2.0$, $a_j/h=0.05$]

4.5. Effect of the wall draft

Most wave power is concentrated at no more than a quarter wavelength below the sea water level, hence the wall draft of the platform is one of the key factors affecting its power extraction and wave attenuation. Fig. 11 shows wave power absorption efficiency and wave transmission coefficient of the platform with five different values of d_j/h and $N=2$, $h=10$ m, $l_0/h=2.0$, $a_j/h=0.05$.

Clearly, as plotted in Fig. 11, smaller d_j/h leads to higher peaks and greater bandwidth of the η - kh curves. The kh values corresponding to these peaks shift towards larger wave frequencies as d_j/h decreases. For long waves, e.g., $kh \in (0, 1.0)$, the effect of the wall draft can be neglected. For $kh=6.8$, no power can be absorbed regardless of the value of d_j/h . For most of the remaining range of the kh , a decrease of the wall draft provides dramatic benefits to the multi-OWC platform for enhancing wave power absorption; however, a decrease of the wall draft goes against wave attenuation of the platform.

Note that, in practice, d_j/h cannot be too small for keeping the platform bottom opening submerged all the time in strong waves and/or large tidal range.

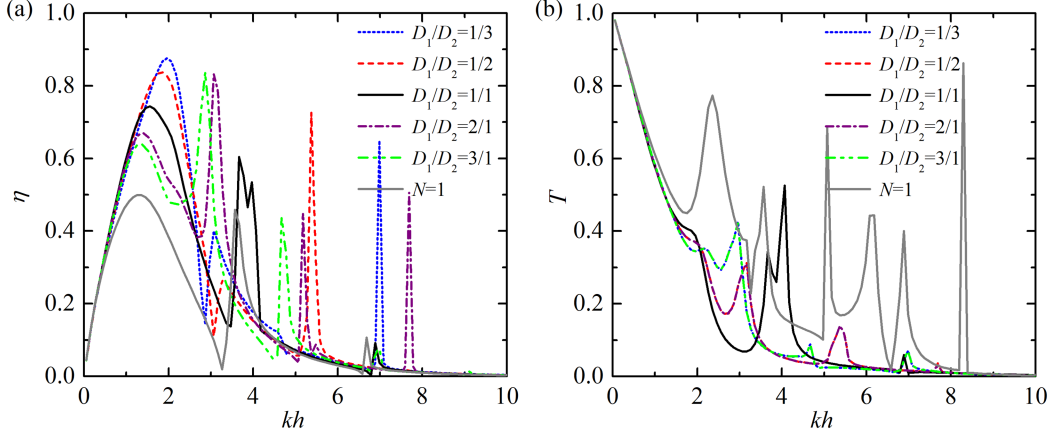


Figure 12: Frequency response of wave power absorption efficiency and wave transmission coefficient for different width ratio of adjacent chambers, i.e., D_1/D_2 : (a) η ; (b) T . [$N=2$, $h=10$ m, $l_0/h=2.0$, $a_j/h=0.05$, $d_j/h=0.2$]

4.6. Effect of the width ratio of adjacent chambers

For each case examined in the above subsections (i.e., §4.1–§4.5), the OWC chambers involved in the multi–OWC platform have the same geometric dimensions. In this subsection, a platform consisting of two OWC chambers with unequal width (specifically, $D_1/D_2=1/3, 1/2, 1/1, 2/1, 3/1$) is considered with a fixed overall platform length. Analytical results of the power absorption efficiency and wave transmission coefficient for these five cases with different values of D_1/D_2 are given in Fig. 12, in which the results of the single–chamber platform without the intermediate wall are also plotted as a comparison.

The existence of the intermediate wall in the platform is found to influence the power absorption of the platform significantly, especially the main peak in terms of peak values and the kh where the main peak occurs. For $N=1$, the main peak value of η and the corresponding kh are $(0.50, 1.36)$, whereas for $N=2$ with $D_1/D_2=1/3, 1/2, 1/1, 2/1, 3/1$, they are $(0.88, 1.96)$, $(0.84, 1.86)$, $(0.74, 1.56)$ and $(0.67, 1.36)$ and $(0.64, 1.36)$, respectively. As the intermediate wall comes close to the leeward edge of the platform (i.e., a larger value of D_1/D_2), the results are close to those of the single–chamber platform. It is interesting

to note that although the largest main peak value (i.e., 0.88) is achieved at
345 $kh=1.96$ when $D_1/D_2=1/3$, η drops to merely 0.15 at $kh=2.86$, where, on the contrary, the η for $D_1/D_2=3/1$ rises rapidly to the second peak with the value ($\eta=0.84$) even larger than its main peak value ($\eta=0.64$ at $kh=1.36$). Similar circumstances also happen for the comparison between the cases of $D_1/D_2=1/2$ and $D_1/D_2=2/1$ at $kh=3.07$. Hence for real sea states, when wave power is
350 concentrated in a small range of wave frequencies, e.g., most of incident wave power exists at $kh \in (1.0, 2.0)$, the platform with a smaller value of D_1/D_2 is welcome for a better power absorption; while if the incident wave power is distributed in a large range of wave frequencies, e.g., $kh \in (1.0, 3.0)$, or even for bimodal wave spectra, the platform with its larger OWC chamber placed at
355 the front might be beneficial for power extraction.

It is observed from Fig. 12b that the $T-kh$ curves corresponding to any two cases with reciprocal values of D_1/D_2 overlap one another. This interesting finding means that for any two multi-OWC platforms with reciprocal D_1/D_2 (just like the same multi-OWC platforms under the waves propagating in opposite directions), the wave transmission coefficients of these platforms are all the same, though there are generally dramatic differences between the results of the wave power absorption (Fig. 12a). The theoretical proof of such “reciprocity” relation regarding the T is given in Appendix A.
360

4.7. Effect of the draft ratio of adjacent walls

365 Finally, we consider how wave power absorption and wave transmission are affected by the draft ratio of adjacent walls. Five cases with different values of d_1/d_2 (specifically, $d_1/d_2=1/3, 1/2, 1/1, 2/1, 3/1$) are studied in this subsection provided $d_1/d_2=d_2/d_3$ and $d_2/h=0.2$. Results of the wave power absorption efficiency and wave transmission coefficient of these cases are illustrated in Fig.
370 13.

It can be observed from Fig. 13a that d_1/d_2 plays a dominant role in affecting the performance of the platform in capturing wave power. For most wave conditions in the computed range of kh , especially for $kh \in (0.5, 3.0)$,

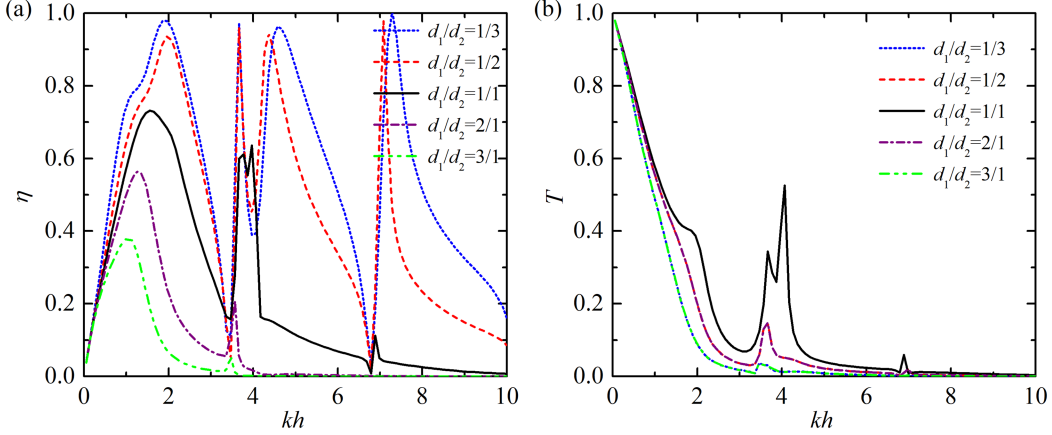


Figure 13: Frequency response of wave power absorption efficiency and wave transmission coefficient for different draft ratio of adjacent walls, i.e., $d_1/d_2 = d_2/d_3$: (a) η ; (b) T . [$N=2$, $h=10$ m, $l_0/h=2.0$, $a_j/h=0.05$, $d_2/h=0.2$]

$kh \in (4.5, 6.5)$, and $kh \in (7.4, 10.0)$, as d_1/d_2 increases from $1/3$ to $3/1$, the η decreases dramatically. For some specified cases, almost all the incident power can be absorbed at certain wave conditions, e.g., $kh=1.9$ and 7.3 for the case with $d_1/d_2=1/3$. On the contrary, $\eta \approx 0.0$ is obtained for the multi-OWC platform with $d_1/d_2=2/1$ and $3/1$ when $kh \in (4.0, 10.0)$. This is reasonable because most wave power is concentrated near the free surface, and if d_1/h (associated with d_1/d_2 in this subsection) is large enough or the wave length is small enough, all incident waves can be reflected from the front wall of the platform back to the sea, leading to no power absorption. For d_1/d_2 with a rather small value, e.g., $d_1/d_2=1/3$, compared to the cases with $d_1/d_2 \geq 1/1$, on the one hand, incident waves are more easily able to enter the OWC chambers of the platform due to a smaller d_1 ; on the other hand, more power can be reflected from the back wall (less power can be transmitted through the back wall) due to a larger d_2 , leading to a significant enhancement of wave power extraction.

A further observation arises from the comparison between the results of $d_1/d_2=1/3$ and $d_1/d_2=3/1$. Note that the main peak for $d_1/d_2=3/1$ occurs at $kh=1.06$. For $d_1/d_2=1/3$, although the main peak happens at $kh=1.86$, the

power extraction is also strengthened at $kh=1.06$ which is associated with the main peak for $d_1/d_2=3/1$. Similar results can also be observed in the comparison between the results for $d_1/d_2=1/2$ and $2/1$. It means that adopting a smaller-draft front wall and a larger-draft back wall provides benefits for broadening
395 the range of high-efficiency performance of the platform.

As expected from the proof given in Appendix A, the $T-kh$ curves corresponding to any two cases with reciprocal values of d_1/d_2 overlap with each other (Fig. 13b). For any specified wave condition in the computed range of
400 kh , the more uneven of the wall drafts, the smaller the transmission coefficient can be obtained.

5. Conclusions

A multi-OWC integrated offshore stationary platform, which works not only as a wave energy device to extract wave power but also as a breakwater to attenuate water waves is proposed. To assess the wave power absorption and
405 wave transmission of the multi-OWC platform, a semi-analytical approach is developed based on linear potential flow theory and an eigen-function expansion method without the assumption of thin-wall and shallow draft. Therefore, the model enables us to explore properties of the platform that would not be possible using simpler models.

410 The results of wave excitation volume flux and hydrodynamic coefficients predicted by using the two different solution methods are in excellent agreement and the energy conservation relationship is satisfied perfectly, giving confidence in the present semi-analytical model for solving wave diffraction/radiation problems, and evaluating wave power absorption and wave transmission of the multi-OWC platform.
415

The validated semi-analytical model is then applied to investigate the effects of a range of parameters, such as the PTO strategies, the number of chambers, the overall platform dimensions and the relative dimensions of adjacent chambers, on the power extraction and wave attenuation of the multi-OWC platform.

⁴²⁰ The following conclusions may be drawn:

- For a multi–OWC platform with identical OWC chambers, no wave power can be captured when $kD_j = 2\pi$ is satisfied, regardless of the three PTO strategies examined.
- ⁴²⁵ - As the number of chambers increases, the wave power extraction from the platform is improved in terms of both a larger peak value and a larger bandwidth of the main η – kh peak. The multi–OWC platforms with $N=4$ and 5 rarely transmit the short incident waves.
- ⁴³⁰ - The peaks of the η – kh curve shift towards the smaller wave frequencies and the peak values increase with the increase of the platform overall length. For long waves, e.g., $kh \in (0, 2.0)$, the transmission coefficient decreases with the increase of the length of the platform.
- ⁴³⁵ - The multi–OWC platform with thinner walls has better performance in terms of wave power extraction for most of the computed range of wave conditions; however, from the view of wave attenuation, the multi–OWC platform with thicker walls is better since smaller values of wave transmission coefficient are generally obtained.
- ⁴⁴⁰ - For most wave conditions, a decrease of the wall draft provides dramatic benefits to the multi–OWC platform for enhancing wave power absorption; however, a decrease of the wall draft goes against wave attenuation of the platform.
- For a platform consisting of two OWC chambers, as the intermediate wall of comes close to the leeward edge of the platform, the results of η become close to those of the single–chamber platform.
- ⁴⁴⁵ - Adopting a smaller–draft front wall and a larger–draft back wall is beneficial for broadening the range of high–efficiency performance of the platform.

- It has been proven theoretically that a multi–OWC platform encountering waves from opposite directions leads to the same transmission coefficient.

The semi-analytical model developed in this paper can be further extended
⁴⁵⁰ to study the performance of a floating multi–OWC platform. The viscous effects which induce vortex shedding at the lips of the walls are neglected. These effects should be considered in order to obtain more realistic prediction of the platform’s performance, especially for extreme wave conditions (Wang et al., 2018; Wang and Ning, 2020).

⁴⁵⁵ **Acknowledgements**

The research was supported by Intelligent Community Energy (ICE), INTERREG V FCE, European Commission (Contract No. 5025), and Open Research Fund Program of State Key Laboratory of Coastal and Offshore Engineering, Dalian University of Technology (LP1928). The corresponding author
⁴⁶⁰ gratefully acknowledges the financial support from China Scholarship Council (Grant No. 201806060137).

Appendix A. Proofs of the same transmission coefficient for two multi–OWC platforms with inverse geometric constructions

⁴⁶⁵ For convenience, the comparison between two multi–OWC platforms with inverse geometric constructions can be transformed into the hydrodynamic problems of a multi–OWC platform suffering from the waves with incoming angle equal to 0 and 180 degree, respectively.

The complex wave transmission coefficient for the opposite coming waves corresponding to Eq. (29) is given by

$$\hat{T}' = \hat{T}'_0 + \frac{i\omega}{gA} Z_1(0) \dot{\mathbf{X}}'^T \mathbf{A}^-, \quad (\text{A.1})$$

in which $\dot{\mathbf{X}}'$ is the air pressure response vector of the multi–OWC chamber with
⁴⁷⁰ waves incoming from the opposite direction; and \hat{T}'_0 denotes the corresponding

complex transmission coefficient of the non-deck multi-OWC platform for the opposite coming waves as well.

For 2D wave diffraction problem of the multi-OWC platform when the dynamic air pressure is zero for all OWCs, the complex transmission coefficient of the platform is found to be the same as that when it suffers from waves propagating in the opposite direction (Falnes, 2002; Newman, 1976), i.e.,

$$\hat{T}'_0 = \hat{T}_0. \quad (\text{A.2})$$

Following Eq. (23), the wave excitation volume flux vectors corresponding to wave incoming angles 0 and 180 degree can be expressed as

$$\mathbf{F}_e = \frac{2i\rho g A k h \mathbf{A}^-}{Z_1(0)} \text{ and } \mathbf{F}_e' = \frac{2i\rho g A k h \mathbf{A}^+}{Z_1(0)}, \quad (\text{A.3})$$

respectively.

With the employment of Eqs. (25) and (A.3), we have

$$\dot{\mathbf{X}}^\top \mathbf{A}^+ = \mathbf{F}_e^\top (\mathbf{S}^{-1})^\top \mathbf{A}^+ = \frac{2i\rho g A k h}{Z_1(0)} (\mathbf{A}^-)^\top (\mathbf{S}^{-1})^\top \mathbf{A}^+, \quad (\text{A.4})$$

and

$$\dot{\mathbf{X}}'^\top \mathbf{A}^- = \mathbf{F}_e'^\top (\mathbf{S}^{-1})^\top \mathbf{A}^- = \frac{2i\rho g A k h}{Z_1(0)} (\mathbf{A}^+)^T (\mathbf{S}^{-1})^\top \mathbf{A}^-, \quad (\text{A.5})$$

where $\mathbf{S} = -i(\mathbf{M}_a + \mathbf{M}_{PTO}) + (\mathbf{C}_d + \mathbf{C}_{PTO})$.

Because of the symmetry of the matrix \mathbf{S} , we have $(\mathbf{S}^{-1})^\top = \mathbf{S}^{-1}$. Moreover, note from Eqs. (A.4)–(A.5) that both $\dot{\mathbf{X}}^\top \mathbf{A}^+$ and $\dot{\mathbf{X}}'^\top \mathbf{A}^-$ are scalars, hence they equal their own transpose. By transposing Eq. (A.4) or (A.5), we have

$$\dot{\mathbf{X}}^\top \mathbf{A}^+ = \dot{\mathbf{X}}'^\top \mathbf{A}^-. \quad (\text{A.6})$$

Utilizing Eqs. (29), (A.1), (A.2) and (A.6), the following equation can be obtained,

$$\hat{T}' = \hat{T}, \quad (\text{A.7})$$

⁴⁷⁵ which theoretically demonstrates that a multi-OWC platform suffering from waves in opposite directions leads to the same transmission coefficient.

References

- Bellew, S., Stallard, T., Stansby, P., 2009. Optimisation of a heterogeneous array of heaving bodies, in: Proceedings of the 8th European Wave and Tidal Energy Conference, pp. 519–527.
480
- Bozzi, S., Giassi, M., Miquel, A.M., Antonini, A., Bizzozero, F., Gruosso, G., Archetti, R., Passoni, G., 2017. Wave energy farm design in real wave climates: the Italian offshore. *Energy* 122, 378 – 389.
- Bozzi, S., Miquel, A.M., Antonini, A., Passoni, G., Archetti, R., 2013. Modeling of a point absorber for energy conversion in Italian seas. *Energies* 6, 3033–3051.
485
- Evans, D.V., Porter, R., 1995. Hydrodynamic characteristics of an oscillating water column device. *Applied Ocean Research* 17, 155–164.
- Falnes, J., 2002. Ocean waves and oscillating systems: linear interactions including wave-energy extraction. Cambridge university press.
490
- Falnes, J., McIver, P., 1985. Surface wave interactions with systems of oscillating bodies and pressure distributions. *Applied Ocean Research* 7, 225–234.
- Gaeta, M.G., Segurini, G., Moreno, A.M., Archetti, R., 2020. Implementation and validation of a potential model for a moored floating cylinder under waves.
495
- Journal of Marine Science and Engineering* 8, 131.
- He, F., Huang, Z., 2014. Hydrodynamic performance of pile-supported OWC-type structures as breakwaters: An experimental study. *Ocean Engineering* 88, 618–626.
- He, F., Huang, Z., Law, A.W.K., 2013. An experimental study of a floating
500
- breakwater with asymmetric pneumatic chambers for wave energy extraction. *Applied Energy* 106, 222–231.

- He, F., Leng, J., Zhao, X., 2017. An experimental investigation into the wave power extraction of a floating box-type breakwater with dual pneumatic chambers. *Applied Ocean Research* 67, 21–30.
- 505 He, F., Zhang, H., Zhao, J., Zheng, S., Iglesias, G., 2019. Hydrodynamic performance of a pile-supported OWC breakwater: An analytical study. *Applied Ocean Research* 88, 326–340.
- Konispoliatis, D.N., Mavrakos, S.A., 2016. Hydrodynamic analysis of an array of interacting free-floating oscillating water column (OWC's) devices. *Ocean Engineering* 111, 179–197.
- 510 Konispoliatis, D.N., Mavrakos, S.A., 2019. Theoretical performance investigation of a vertical cylindrical oscillating water column device in front of a vertical breakwater. *Journal of Ocean Engineering and Marine Energy* , 1–13.
- Newman, J.N., 1976. The interaction of stationary vessels with regular waves,
515 in: *Proceedings of the 11th Symposium on Naval Hydrodynamics*, London, 1976, pp. 491–501.
- Ning, D., Wang, R., Chen, L., Sun, K., 2019. Experimental investigation of a land-based dual-chamber owc wave energy converter. *Renewable and Sustainable Energy Reviews* 105, 48–60.
- 520 Ning, D., Zhou, Y., Zhang, C., 2018. Hydrodynamic modeling of a novel dual-chamber OWC wave energy converter. *Applied Ocean Research* 78, 180–191.
- Noad, I., Porter, R., 2017. Wave energy absorption by a shallow-draughted rectangular barge of oscillating water columns, in: *Proceedings of the 12th European wave and Tidal energy Conference*. 27th Aug–1st Sept, 2017, Cork, Ireland, pp. 1–9.
- Pereiras, B., López, I., Castro, F., Iglesias, G., 2015. Non-dimensional analysis for matching an impulse turbine to an OWC (oscillating water column) with an optimum energy transfer. *Energy* 87, 481–489.

- Rezanejad, K., Bhattacharjee, J., Guedes Soares, C., 2016. Analytical and
530 numerical study of nearshore multiple oscillating water columns. *Journal of Offshore Mechanics and Arctic Engineering* 138, 021901.
- Rezanejad, K., Bhattacharjee, J., Soares, C.G., 2013. Stepped sea bottom effects on the efficiency of nearshore oscillating water column device. *Ocean Engineering* 70, 25–38.
- 535 Rezanejad, K., Bhattacharjee, J., Soares, C.G., 2015. Analytical and numerical study of dual-chamber oscillating water columns on stepped bottom. *Renewable Energy* 75, 272–282.
- Rezanejad, K., Soares, C.G., López, I., Carballo, R., 2017. Experimental and
540 numerical investigation of the hydrodynamic performance of an oscillating water column wave energy converter. *Renewable Energy* 106, 1–16.
- Sarmento, A.J.N.A., Falcão, A.F.d.O., 1985. Wave generation by an oscillating surface-pressure and its application in wave-energy extraction. *Journal of Fluid Mechanics* 150, 467–485.
- Sheng, W., 2019. Motion and performance of bbdb owc wave energy converters:
545 I, hydrodynamics. *Renewable Energy* 138, 106–120.
- Wang, R., Ning, D., 2020. Dynamic analysis of wave action on an OWC wave energy converter under the influence of viscosity. *Renewable Energy* 150, 578–588.
- Wang, R., Ning, D., Zhang, C., Zou, Q., Liu, Z., 2018. Nonlinear and viscous effects on the hydrodynamic performance of a fixed OWC wave energy
550 converter. *Coastal Engineering* 131, 42–50.
- Zheng, S., Antonini, A., Zhang, Y., Greaves, D., Miles, J., Iglesias, G., 2019a. Wave power extraction from multiple oscillating water columns along a straight coast. *Journal of Fluid Mechanics* 878, 445–480.

- 555 Zheng, S., Zhang, Y., 2016. Wave diffraction and radiation by multiple rectangular floaters. *Journal of Hydraulic Research* 54, 102–115.
- Zheng, S., Zhang, Y., 2017. Analysis for wave power capture capacity of two interconnected floats in regular waves. *Journal of Fluids and Structures* 75, 158 – 173.
- 560 Zheng, S., Zhang, Y., 2018. Analytical study on wave power extraction from a hybrid wave energy converter. *Ocean Engineering* 165, 252–263.
- Zheng, S., Zhang, Y., Iglesias, G., 2019b. Coast/breakwater-integrated OWC: A theoretical model. *Marine Structures* 66, 121–135.
- Zheng, S., Zhu, G., Simmonds, D., Greaves, D., Iglesias, G., 2020. Wave power extraction from a tubular structure integrated oscillating water column. *Renewable Energy* 150, 342–355.